Genetic Algorithm applied to the optimized design of semiconductor microcavity lasers

Fernando C. da Silva Coelho[1,3], E. A. Cotta[*2,3] and Omar P. Vilela Neto[1,3]

[1]Universidade Federal de Minas Gerais, Departamento da Ciência da Computação - Belo Horizonte, Brazil
[2]Universidade Federal do Amazonas, Departamento de Física - Manaus, Brazil
[3]Instituto Nacional de Ciência e Tecnologia de Nanodispositivos Semicondutores (INCT:DISSE) - Rio de Janeiro, Brazil
*cotta@ufam.edu.br

ABSTRACT

Semiconductor microcavities have been used in important studies of several areas for technological or purely scientific purposes. However, the definition of the optimal parameters for the fabrication of microcavities is a difficult task. Moreover, some uncertainties related to the growth process can change the device features. These problems cannot be experimentally controlled, hindering the development of theoretical models. In this work we present a theoretical model to simulate the microcavities and also propose an evolutionary approach to optimize the device under uncertainty in order to ensure the growth with the desired features. Thus, based on the reflectance spectra of a $Al_xGa_{1-x}As$ semiconductor microcavity, the aluminum concentrations, x, and the number of layers that compose the heterostructure were optimized. This set of parameters may offer increased robustness in the growth process, while providing a considerable quality factor and the desired position of the cavity resonance, achieving the device's operation limits. The device was optimized considering the cavity resonance between 700nm and 2000nm, where the results indicate that the proposed algorithm is able to find satisfactory solutions, minimizing the problems caused by inaccuracy in the growth process.

Index Terms: *microcavity; genetic algoritm; laser; reflectance spectrum;* $Al_xGa_{1-x}As$.

I. INTRODUCTION

In the last two decades, the semiconductor microcavities have been used for technological or purely scientific purposes. Ideally, a microcavity is a system in which a light-emitting material can interact with a single cavity-resonant-mode or no interactive electromagnetic modes within the material transition width. Thus, enhanced or suppressed spontaneous emission can be seen in this system, and in a cavity with a very high quality factor Q, an even spontaneous oscillatory emission can be induced [1,2].

Among the recent studies performed in microcavities we can emphasize: (a) the development of low threshold emission lasers, since microcavities act as a laser without population inversion [3]; (b) construction of optical transistors [4] and other optical devices [5] (c) a parametric generator of twin photons through parametric up- or down-conversion process [6,7] (d) the Bose-Einstein condensate of exciton-polaritons [8]; (e) effects of fully controllable optical bistability [9], among many others.

In a typical sample, a gain medium is placed at antinodes of a cavity formed by two Diffracted Bragg Reflector (DBR) mirrors and kept at cryogenic temperatures. During the growth process, usually by Molecular Beam Epitaxy technique (MBE), the sample rotates to ensure uniformity of the layer and minimize the roughness on the interfaces. At a specific angle, the rotation is stopped to grow the spacer layer that generates a thickness gradient across the sample. This allows the user to make a cavity-detuning when exciting the sample in different positions on the surface. The Q factor of the cavity can be measured directly using an unpolarized white light source, focusing normally on the sample surface.

In order to synthesize devices with the desired features, it is required an excellent coupling between the resonance cavity and the gain medium, which mainly consist of quantum-well(s) or quantum-dots. Thus, it is very important to find an exact coupling between the cavity-resonance and the emission peak of the gain media. Therefore, beyond an architectural design project, a precise control of the growth becomes essential to take advantage from the optical properties of the sample materials.

In this sense, a deep understanding of the effects of many layers that constitute the heterostructure allows computational design of samples in order to know, for example, their reflectance spectrum. Thus, even using materials engineering for the proposed new architectures, there is no way to determine if the design of the sample reached its optimal properties. Moreover, despite the growth of semiconductor nanodevices is well established, some small calibration errors can occur due to small uncertainties in the rates of materials deposition during synthesis. This can lead to the development of nanometer devices with layers thickness slightly different than expected. A semiconductor microcavity typically has tens of layers and these variations can generate problems in the final device operation. For this reason, in this work we performed the optimization of nanodevices considering the uncertainties that may occur, in order to find the optimal parameters that can lead to the fabrication of robust devices, despite uncertainties involved. The optimization of the parameters will be evaluated analyzing the reflectance spectrum of the heterostructure, where the main objective is to find an architecture in which the cavity resonance is positioned in a desired point, but with the best Q factor.

To solve the uncertainty problem, we are proposing a computational method using a Genetic Algorithm (GA) in order to optimize the architectures of microcavities based on semiconductor technology for the ternary alloy of $Al_xGa_{1-x}As$ while maintaining robustness. To the best of our knowledge, it is the first time that this optimization procedure is proposed for these structures.

In our model, the microcavity to be optimized present a 10nm of GaAs single quantum well (SQW) positioned on the center of a λ-cavity. Thus, with these characteristics the SQW presents an emission peak about 800nm and, in this position, it is on the anti-node of the cavity normal mode, increasing the coupling between the SQW and the cavity photon. Thus, our purpose is to design a microcavity based in $Al_xGa_{1-x}As$ alloy that shows the position of the spectral resonance fixed in the desired value by the designer (on the emission peak of the gain medium). Furthermore, the algorithm must maximize the cavity quality factor (Q), but without significantly burdening the growth process. We have optimized microcavities with resonance peak between 700nm and 2000nm with steps of 100nm. The results show that our proposed method is efficient in order to find the optimized set of parameters that allow the growth of the desired nanodevice even under experimental doubt.

This paper is organized as follow: section II presents the model to simulate the reflectance spectra in microcavities and that had been applied in the optimization process; section III describes the optimization problem and presents the algorithm details; section IV presents and discusses the results. Finally, concluding remarks are given in Section V.

II. MICROCAVITIES SIMULATION: THE REFLECTANCE SPECTRA

The schematic of the microcavity structure that will be considered in this work is presented in Fig. 1. In this figure we can see that the heterostructure is grown on the top of a GaAs substrate oriented in the direction ⟨100⟩. Alternating layers of two different materials based on ternary alloy of $Al_xGa_{1-x}As$ are deposited on the substrate, where x is the concentration of aluminum. The deposition of the first two layers gives rise to the pair that is presented in the figure by white (refractive index n_1 and thickness l_1) and light gray (refractive index n_2 and thickness l_2). The periodic superposition of N_1 pairs of layers creates a DBR mirror (Distributed Bragg Reflector) at the bottom of the sample. Also, an upper DBR mirror with N_2 pairs of layers in formed. The two DBR mirrors are separated by a spacer layer (refractive index n_3 and thickness l_3) also of $Al_xGa_{1-x}As$, forming a Fabry-Perot cavity type. A single quantum well (SQW) of GaAs, 10nm thick, is placed in the middle of the cavity.

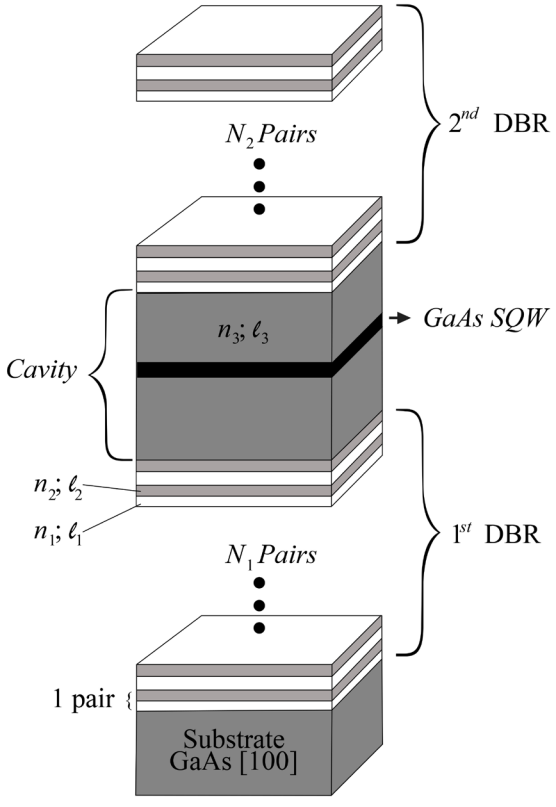

Figure 1. Schematic microcavity's structure to be optimized.

To model the reflectance spectra of a microcavity heterostructure we apply the transfer matrix technique, where the transfer matrix for the i^{th} layer with thickness l_i, have the following format [10]:

$$M = \begin{bmatrix} \cos\varphi_i & -\frac{i}{p}\sin\varphi_i \\ -ip\sin\varphi_i & \cos\varphi_i \end{bmatrix} \quad (1)$$

where $\varphi_i = k_i l_i \cos\theta_i$ is the phase accumulated by the light to pass through the i^{th} layer, being θ_i the refracted angle by this layer, that is related to incident angle θ_0 by Snell Law, and

$$p = (n_i \cos\theta_i)\cos\phi + \left(\frac{n_i}{\cos\theta_i}\right)\sin\phi \quad (2)$$

defines the polarization component for incident light on the surface sample. Here, n_i is the refractive index of the i^{th} layer, $k_i = 2\pi n_i/\lambda_0$ is the wavevector, λ_0 is the vacuum wavelength. In this case, an arbitrary linear polarization state is described by angleϕ, in which the TE polarization is given to $\phi = 0$ an TM to $\phi = \pi$.

For N layers the total transfer matrix M is given by the product of individual layer matrices:

$$M = M_1 M_2 M_3 ... M_N = \begin{bmatrix} A & B \\ C & D \end{bmatrix} \quad (3)$$

The coefficients A, B, C and D in eq. 3 are used to determine r and t coefficients, where:

$$r = \frac{A\cos\theta_0 n_0 + B\cos\theta_0 n_0 \cos\theta_T n_T - C - D\cos\theta_T n_T}{A\cos\theta_0 n_0 + B\cos\theta_0 n_0 \cos\theta_T n_T + C + D\cos\theta_T n_T} \quad (4\text{-a})$$

and

$$t = \frac{2\cos\theta_0 n_0}{A\cos\theta_0 n_0 + B\cos\theta_0 n_0 \cos\theta_T n_T + C + D\cos\theta_T n_T}, \quad (4\text{-b})$$

where n_T and θ_T are the refractive index and the refracted angle of the transmission medium, respectively. The transmittance and reflectance spectra are given by $T = |t|^2$ and $R = |r|^2$.

The semi-classical theory for light propagation in a dielectric applies the Lorentz model [11] in which the electrons are considered damped harmonic oscillators driven by an external electric field. In order, the solution for the general wave equation for **E** (a homogeneous plane harmonic wave), provide us a complex refractive index $\eta = n + i(c/\omega)\alpha$, where the real part ($n$) provides the dispersion behavior of the medium and can be described by first-order Sellmeier equation [12]:

$$n^2(\lambda, x) = A(x) + \frac{B(x)\lambda^2}{\lambda^2 - C(x)}, \quad (5)$$

where the coefficients $A(x)$, $B(x)$ and $C(x)$ are fitting parameters, but now dependent of Aluminum concentration x in the $Al_xGa_{1-x}As$ ternary alloy. In this model, the contribution to the decrease of the refractive indexes due to lattice absorption is neglected. The imaginary part of the complex refractive index η is known as the extinction index, and and 2α is the absorption's coefficient of the medium (c and ω are the vacuum light speed and the frequency, respectively).

The refractive index of $Al_xGa_{1-x}As$ has been widely measured for a certain range of wavelenghs [13], around the gap energy, and for specific multi-quantum well structures [14,15]. However, a general model to the optical dispersion of this alloy is necessary, and important material parameters may be found in order to design many optoelectronic devices. Thus, using the known experimental data for the refractive index of several values of x at 300K for $Al_xGa_{1-x}As$ alloy [13], we applied an empirical fitting from Eq. (5) to obtain Sellmeier's coefficients as a function of x. The coefficients are fitted by a low order polynomial, passing through as many points as possible.

Since excitons provide a sensitive indicator of material quality, the high exciton binding energies found in these alloys are especially interesting. The mechanisms that broaden or shift the exciton resonance, such as doping, strain, and phonon interactions, also broaden and shift the absorption edge. These effects influence the optical constants near the band gap. The description of optical absorption of semiconductors near the band edge, allowing the Coulomb interaction between electrons and holes, for the consequent formation of excitons has been worked out in the effective mass approximation by Elliott [16].

For the simple non-degenerate parabolic bands at the center of the Brillouin zone, in which transitions are direct and parity-allowed, the absorption coefficient in the region of continuous absorption is given by [16]:

$$\alpha = \frac{8\pi^2\varepsilon|P_{cv}|^2}{\lambda n(\omega) a_0}\frac{1}{1-e^{2\pi z}} \quad (6)$$

for

$$z^2 = \frac{E_x}{E - E_g}, \quad (7)$$

where $E(\lambda)$ is the incident photon energy (wavelength), E_g is the energy gap, $E_x = 2\mu e^4/(8\pi\hbar\varepsilon)^2$ is the exciton binding energy for 1s-state, ε is the dielectric constant

and $a_0 = 4\pi\varepsilon\hbar^2/(\mu e^2)$ is the Bohr radius. Moreover, $\mu^{-1} = m_e^{-1} + m_h^{-1}$, where m_e and m_h are the electron and hole mass, respectively. The momentum matrix element at $k = 0$ is defined as $P_{cv} = \langle \psi_{c,0} | p | \psi_{v,0} \rangle$ in which the strength of optical transitions is determined, and also governs the electromagnetic interaction with electrons and solids. The energy band curvature diagrams provide important information on the strength of optical transitions. Correspondingly, knowledge of the optical properties can be used to infer experimental information about $E(\lambda)$. Thus, $|P_{cv}|^2$ give us the transitions dependence on the coupling between the valence and conduction bands and this is measured by the magnitude of the momentum matrix elements coupling the valence band state, described by $\psi_{v,0}$, and the conduction band state, described by $\psi_{c,0}$ and, therefore, must reflect the bands curvatures. Consequently, we include the band curvature in $|P_{cv}|^2$, where around of the Brillouin zone center ($k = 0$: Γ point) this curvature is approximately parabolic.

However, it is know that $Al_xGa_{1-x}As$ ternary alloy undergo a direct-to-indirect gap transition when the Al concentration is $x \geq 0.45$. In this case (for $x \geq 0.45$), the absorption is given by [17]

$$\alpha = \frac{8\pi^2 \varepsilon |2\beta P_{cv}|^2}{3a_0^4 \lambda n(\omega)} \frac{1+z^{-2}}{1-e^{-2\pi z}}, \qquad (8)$$

where β is the nearest neighbors distance. Moreover, in the case where the incident photon has energy below the gap energy, the absorption coefficient is given by [16]

$$\alpha = \alpha_0 \exp\left[\sigma_0 \left(\frac{E-E_g}{E}\right) \tanh\left(\frac{E}{2k_B T}\right)\right], \qquad (9)$$

where α_0 is given by (7) or (9) for $E = E_g$. The steepness parameter, σ_0, is independent of the incident photon energy and is a temperature-independent constant proposed to be inversely proportional to the exciton-phonon interaction strength [18]. In our purpose, σ_0 is Aluminum concentration dependent and have a polynomial behavior with x.

Based in these considerations, we have reused the experimental data presented by Sadao Adashi [13] for the extinction coefficient and the refractive index for $Al_xGa_{1-x}As$ to obtain a set of parameters for the generalized model. Our approach was validated by a superposition of a measurement of the reflectance spectra and the corresponding theoretical curve (see Fig. 2a). In this figure, we present the results for a microcavity grown over a *GaAs* [100] insulating substrate, containing 22 pairs of $AlAs/Al_{0.2}Ga_{0.8}As$ in the bottom DBR, and 26 pairs in the top DBR. The λ-cavity is composed by $Al_{0.3}Ga_{0.7}As$. Our model corroborates very well with experimental data, where the resonance position have a great accuracy, validating it. The theoretical stop-band seems to be larger than the experimental measurement due to imperfections in the thickness of the constituent layers of the DBR mirrors. Despite the theoretical fitting presents a transmittance higher than the experimental in the resonance, the quality factors are the same in both cases. Fig. 2b presents an experimental spectrum for a microcavity with resonance peak in 912nm, where the DBR mirrors are made of $GaAs/Al_{0.3}Ga_{0.7}As$ with 30 pairs in the bottom and 26 pairs in the top. The λ-cavity was made of *GaAs*, where a high transmission on the cavity resonance and an increasing in the Q factor to 1150 are observed. This structure was not used in the validation of the theoretical model because serious growth problems were reported during the synthesis. So, we cannot guarantee that the parameters are correct.

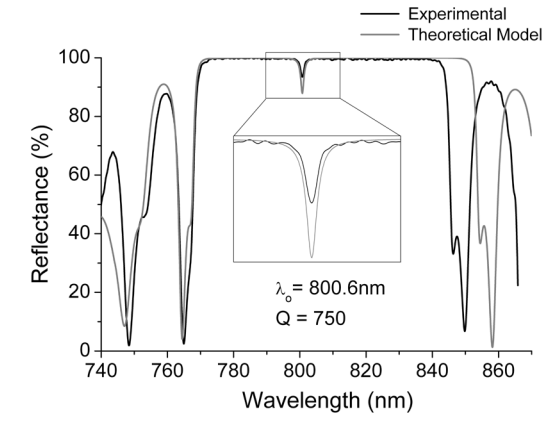

(a)

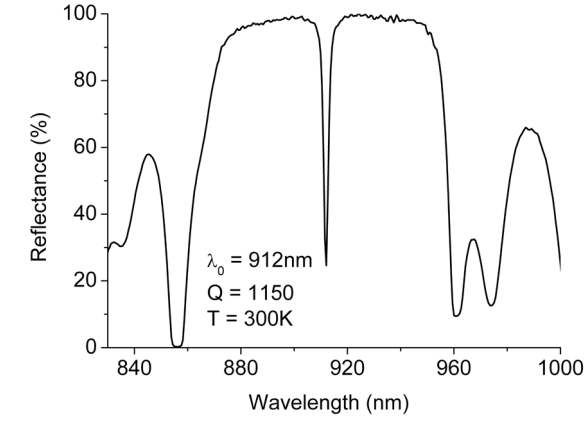

(b)

Figure 2. (a) Superposition of experimental (black line) and theoretical (gray line) reflectance spectra of a microcavity sample with resonance in 800nm. (b) Experimental reflectance spectra for a microcavity with resonance in 912nm. The characteristics of the samples are presented in the text.

III. THE OPTIMIZATION PROCESS

As it has been discussed earlier, the synthesis of semiconductor nanodevices, such as microcavities, is a challenging task because in order to create the desired device the correct set of parameters must be chosen. In this work we are looking for a microcavity with the highest possible Quality Factor (Q) and the correct position of cavity's resonance peak (λ_o).

Quality Factor ($Q = \Delta\lambda/\lambda_o$) is measured from the reflectance spectra, where the full width at half maximum (FWHM) of the resonance ($\Delta\lambda$) and the cavity resonance position (λ_o) are obtained directly.

It is well known that the resonance peak position is directly related to the thickness of the cavity layer. So, if a particular position of the resonance peak is desirable, the thickness of the cavity layer is easily defined by $L_c = m(\lambda_o/2n_c)$, for an integer number m and a cavity with refractive index n_c. Moreover, the thickness of the layers in the DBR mirror is given by $L_{DBR} = \lambda_o/4n_i$, where n_i is the refractive index of each layer. However, the remaining parameters can slightly shift the resonance energy peak position from the desired value. So, this displacement error, defined as $\Delta E = |E_{desired} - E_{obtained}|$, shall be minimized.

The major challenge for designers is to find the best set of parameters before the experimental synthesis of the desired nanodevice. Such parameters will guide the specialist in the slow and expensive growth process. Whereas the relationship between the desired position of the resonance peak and the thickness of the layers are well known, the algorithm has to search for the others parameters involved in the growth process. In this way, the parameters involved in the microcavities optimization (MO) problem, as shown in Fig. 1 are: (a) Number of layers in the bottom DBR mirror - N_1; (b) Number of layers in the upper DBR mirror - N_2; (c) Aluminum concentration in the first layer of the pair - x_1; (d) Aluminum concentration in the second layer of the pair - x_2; (e) Aluminum concentration in the spacer layer (cavity) - x_c.

Here, x_1, x_2 and x_c are concentration values, ranging from 0 to 1. The parameters N_1 and N_2 are integer numbers between 0 and 30, which limits were defined to not let the synthesis of the device too expensive.

So, given a microcavity with its desirable resonance peak and a set of parameters to be established, the MO problem consists in choosing the set of parameters, such that the Q is maximized and ΔE is minimized.

In this way, each possible set of parameters (solution) generated by the optimization procedure is simulated by the method described earlier. Given the output of the simulator we are able to calculate the Quality Factor (Q) and the error deviation (ΔE) to the desired position of the resonance peak. These variables are related to the fitness function of the solution by the equation bellow:

$$F = Q\left[1 - \left(\frac{\Delta E}{\Delta E + n}\right)\right] \tag{10}$$

where n is a factor of the importance of ΔE.

This way, the microcavity optimization problem can be summarized as to find the maximum of function F, given by Equation (10). This can be expressed by:

$$Solution = MAX[F] \tag{11}$$

Nevertheless, although the synthesis process of semiconductors nanodevices is well developed, some inaccuracies are not fully controlled by experts. The major inaccuracy during the synthesis process is related to the thickness of the layers and their roughness. The roughness problem can be minimized with the use of Molecular Beam Epitaxy (MBE) technique in the growth process. Since our target devices are in nanometer scale, small variations in layers thickness can significantly impact the final result. Thus, the optimization process developed in this work has to deal with uncertainty. During the growth process two different problems can occur: (a) the MBE used to grow the device is calibrated to a specific deposition rate. This deposition rate defines how many atomic layers are deposited per second. An error up to 1% can occur in this process, leading to a thickness variation in all layers; (b) during the deposition of each layer a local error, also equal to 1%, can happen, causing the device to have layers with different thicknesses.

It has been verified that ΔE is strongly related to the growth inaccuracies and the optimized parameters haven't a great influence in the error, but can slightly minimize it. So, the main feature to be optimized is the Q value, but still considering the ΔE. In this work we set $n = 10$ in equation (10) in order to slightly minimize the influence of ΔE in the fitness function.

In order to deal with this uncertainty, each set of parameters representing a solution has it's fitness evaluated against 10 different microcavities structures, in which the first structure presents layers thickness in the DBR mirror given by $L_{DBR} = \lambda_o/4n_i$, where n_i is the refractive index of each layer, as described earlier. The next nine structures are randomly generated considering the 1% error in calibration phase and the 1% error in the growth of each layer. The decision to use ten structures was due to the time consuming simulations for each solution, and due to a large number of structures to be evaluated.

So, to ensure that the expert will be able to grow a microcavity with the desired features, the MO problem is now redefined as:

$$Solution_{lowest} = MAX[MIN[F_i]]; (i = 1, 2, ..., 10 \quad (12)$$

where F_i is the evaluation of the i^{th} structure. In this case we would like to ensure that the worst structure presents good features, allowing the synthesis of the desired material. This strategy has been named as "Lowest".

Also, the "Average" MO problem (strategy) is defined, and used to be compared with the previous strategy:

$$Solution_{average} = MAX\left[\sum_{i=1}^{10} \frac{F_i}{10}\right] \quad (13)$$

In this case, we expect to find structures with homogeneous results, also overcoming the uncertainty problems. Finally, an optimization problem that does not consider the robustness can be defined as:

$$Solution_{Highest} = MAX[MAX[F_i]]; (i = 1, 2, ..., 10) \quad (14)$$

The result of this optimization problem (namely, "Highest" strategy) can generate the highest possible fitness value, but it does not ensure that the microcavity will present the desired features after the growth process.

A. The Genetic Algorithm

In this work we have applied a Genetic Algorithm (GA) in order to optimize the microcavities. GA is a search and optimization algorithm with wide and successful applications in several areas of science and technology [19]. Differently from other optimization algorithms, GA does not include the calculations of derivatives. It is an iterative algorithm that belongs to a group of techniques inspired in Darwin's natural selection principle. These algorithms use a process based on genetic reproduction to achieve an optimal or sub-optimal solution of a problem. The procedure is as follow: each possible solution in a problem is modeled and codified in a string of bits or symbols. Such structure is known as "chromosome" and each bit or symbol is known as a "gene". Thus, each of these chromosomes represents an individual in a population. In other words, it represents a solution in a pool of possible solutions. These individuals are evaluated according to predetermined criteria, known as fitness function, and receive a score that informs how good a particular individual (solution) is for the problem. In the sequence, individuals are chosen based on their score, in a way that individuals with higher scores have a larger probability of being chosen. The selected individuals are combined and new ones are generated.

There are two main genetic operators responsible to create the new individuals: mutation and crossover. Crossover is the process through which the genetic information from two parents chromosome are combined to generate the new individuals. To avoid stagnation and to maintain population diversity, mutation operators are applied. Normally, the mutation randomly perturbs some of the genes in a chromosome. The new individuals are expected to be better or, at least, as good as their generators. The new individuals replace the ones with low scores, and the process restarts. The procedure is repeated until a stop condition is reached. Each cycle of the algorithm is known as a "generation".

In particular, the Genetic Algorithm proposed in this work, as shown in Fig. 3-a, starts with a random set of individuals whose chromosomes are built according to Fig. 3-b. Each gene in the chromosome holds a floating point value ranging from 0 to 1. The first three genes are the Aluminum concentration, x, of the two layers in the pair of the DBR mirrors and of the cavity layer (see Fig. 1). The last two genes represent the number of pair of layers on each DBR mirror. As discussed before, the number of pairs of layers of each DBR was limited in 30. These individuals are evaluated through a fitness function that applies the simulation described in section 2. Different fitness strategies were used as described by (12), (13) and (14).

The crossover operator applied is described as follow: two individuals are selected from the population, considering their fitness values. They are used to generate a pair of new individuals through crossover procedure where each gene for each son is computed according to:

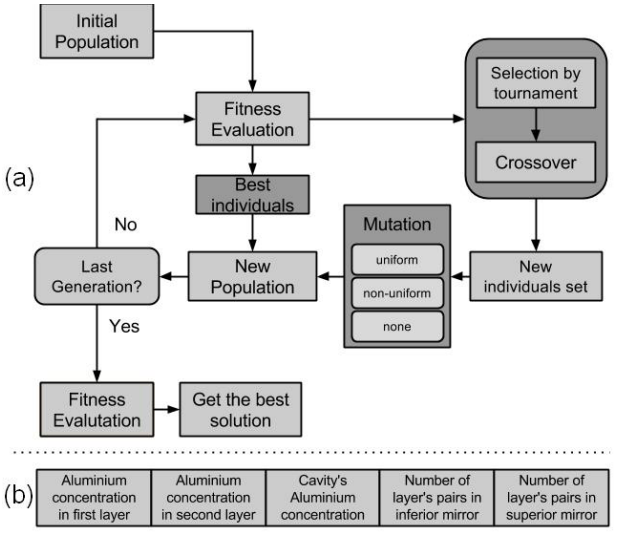

Figure 3. (a) Implemented Genetic Algorithm. (b) Chromosome representing solutions.

$$Son_1 = R*P_1+(1-R)*P_2$$
$$Son_2 = (1-R)*P_1+R*P_2, \quad (15)$$

where R is a random value between 0 and 1 (generated by the algorithm), P_1 and P_2 are the genes of parent 1 and parent 2 of the selected couple, respectively.

After, these new individuals are randomly chosen to perform one of two types of mutation: uniform or non-uniform mutations. These procedures of genetic operators are repeated until a new population is full. In the case of this work, until the algorithm has achieved the defined population size.

The uniform mutation is a process that chooses some genes to receive a new random value, while non-uniform mutation is deeply dependent of how many generations had been done. The non-uniform mutation is a technique to make a fine search and ensure that at least the local optimum is reached [19]. So a gene υ is selected through a mutation rate, and the new value is computed by the equation bellow:

$$\upsilon' = \begin{cases} \upsilon + \Delta(t, UB - \upsilon), \text{ if random value is 0} \\ \upsilon - \Delta(t, \upsilon - LB), \text{ if random value is 1} \end{cases} \quad (16)$$

where t represents the current generation number, LB and UB are the lower and upper bounds domain for variable υ, respectively. $\Delta(t,y)$ returns a value in the range $[0,y]$ that rapidly approaches 0 as the end of generations draws near and is given by

$$\Delta(t,y) = y\left[1 - r^{(1-t/\tau)b}\right] \quad (17)$$

where y is the maximum value that the function can return, r is a random number from [0..1], τ is the maximum generation number, and b is a system parameter determining the degree of dependency on interaction number.

In this way, we allow our search to spread in the space initially and very locally at later stages; thus tuning the search to minor steps, which brings benefits when minimum and maximum can be very near on the search space.

When the algorithm reaches the final generation the GA is stopped, otherwise a new generation (or cycle) begins.

Basing in this model, we have done different experiments with microcavity resonance peaks in the range from 700nm to 2000nm with steps of 100nm. For each resonance peak we have applied three different fitness functions [(12), (13) and (14)], generating a total of 42 experiments. As a stochastic algorithm, for each one we have run 15 seeds, in other words, 15 different GA runs within different random numbers. Each run has a population size of 40 individuals and a total of 200 generations. The elitism is ensured by always copying the best 5 individuals from the last generation to the current generation. The mutation rate is 10% in which we have 50% of uniform mutation and 50% of non-uniform mutation.

IV. RESULTS AND DISCUSSION

In this section we present the results of the optimization process, comparing the proposed strategies. Moreover, we present and discuss how the Quality factor changes with the peak position. Also, a discussion among theoretical results and known experimental results is done.

The results of the best solution found for experiments with resonance peak in 800nm, 900nm and 2000nm are shown in Table 1 (in the Appendix A). The results for the other peaks are not presented due to space limitation, but will be discussed qualitatively. The Table 1 is organized as follow: for each desired peak we present the results for the best solution found by the GA for each fitness strategy (Highest, Average and Lowest evaluation, respectively). The first column, "structure", shows the number of each one of the ten structures used in the fitness calculation. The structure 1 represents the device with the known theoretical thickness of the layers, the following structures represent the randomly thickness simulated microcavities considering the possible growth errors. The column ΔE presents the shift in desired peak position (in *meV*), Q shows the Quality Factor of the structure, and F_i is the evaluation calculated by (10), considering $n = 10$. The last two lines show the mean and standard deviation for ΔE, Q and F_i, respectively. The best mean and standard deviation are shown in bold.

As expected, the three strategies, namely Highest, Average and Lowest evaluation, present the highest F_i, the highest mean F_i, and the highest minimum F_i, respectively. In the best results for the three strategies, all ΔE are small and in the same order of magnitude. The most important conclusion from the results is that the Average and Lowest Evaluation strategies are able to find solutions with high robustness. In other words, we are confident that the expert can apply the set of parameters found to grow the device, once we can see low variation in the ΔE and Q values. Obviously, if we have applied the optimization procedure without considering the uncertainty in the growth process we would not be able to ensure this robustness.

For resonance peak at 800nm and "Highest" strategy, we can observe that the first structure, the one with no random variation in the layers thickness, presents the highest Q = 1600 and $\Delta E = 0$. Only one

of the next nine structures presents a Q close to 1600 while the other structures present Q close to 1330, a reduction of almost 17%. For all these structures the ΔE is small. Looking at the results of the other two strategies ("Lowest" and "Average"), 9 out of 10 structures present Q close to 1600 and small ΔE.

For the resonance peak at 900nm, all structures from fitness strategies "Average" and "Lowest" present a small ΔE and a Q close to 9000, with small variations. On the other hand, 2 out of 10 structures in the "Highest" strategy present a 50% lower Q. In last case, peak at 2000nm, 4 out of 10 structures in the "Highest" strategy show a 50% lower Q and, even worse, structure 6 presents null Q. This confirms that the uncertainty must be taken into account in the optimization process. Despite the results for the other resonance peaks are not explicitly shown here, they follow the same trend.

Figs. 4-a, 4-b and 4-c show the reflectance spectra for the best structures found for resonance peaks at 800nm, 900nm and 2000nm, respectively. The set of parameters needed to build these structures is shown in Table 2.

As can be observed in these reflectance spectra, all resonance peaks are tightly aligned in their respective frequency peaks, as desired in the optimization process. Also, all spectrum presents a very thin peak, which characterizes a good Quality Factor. The spectrum of the optimized microcavity of Figure 4-a can be compared with that of Figure 2-a, showing the huge improvement.

The Table 2 shows all the set of parameters for each resonance peak and strategy presented in this work, which are needed to build structures presented in Table 1.

Naturally, the best optical cavity expected to be generated by the optimization process would have a large number of pairs of layers constituting the DBR mirrors (maximum of 30 allowed in this work) as well as a large difference between the refractive index of the layers constituting the pair. Indeed, one can observe that the aluminum's concentration of one of the two pairs in the DBR mirror are always close to 1 while the other is close to 0. Also, the number of layers is high, but not always 30.

Considering the optimizations of resonance peaks between 700nm and 2000nm, we can see how the Quality Factor changes as a function of the resonance peak. It is remarkable that the best Quality Factor found, after 900nm, increases linearly as the resonance peak increase, as can be seen in Figure 5. In

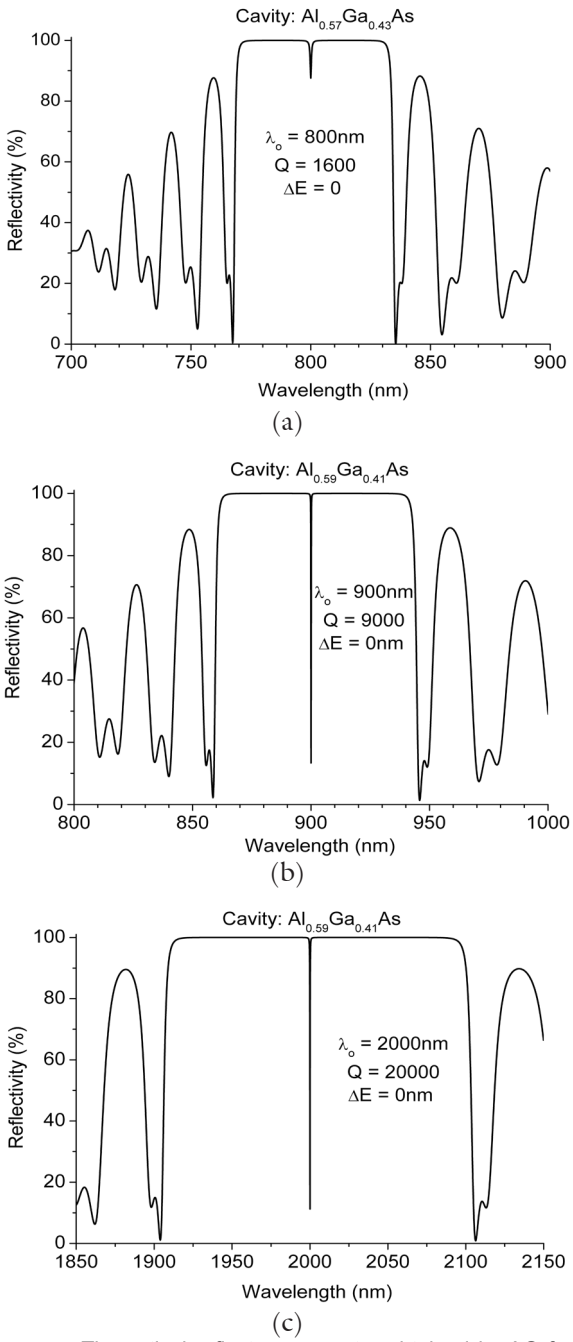

Figure 4. Theoretical reflectance spectra obtained by AG for a microcavity optimised to: (a) 800nm, (b) 900nm and (c) 2000nm. The parameters found in each case are placed in table 2 (Highest Fitness Strategy, structure 1) .

Table II. Best parameters [Aluminum concentration for the cavity (x_c), first (x_1) and second (x_2) layers of the DBR mirror (and the number of pairs of layers in each DBR, N_1 and N_2)] found for the microcavities.

λ_o (*nm*)	Fitness strategy	x_1	x_2	x_c	N_1	N_2
800	Lowest	0.33	0.89	0.58	26	30
	Average	0.35	0.98	0.55	26	30
	Highest	0.28	0.90	0.57	27	28
900	Lowest	0.95	0.07	0.72	27	26
	Average	0.96	0.02	0.78	25	27
	Highest	0.14	0.85	0.59	24	26
2000	Lowest	0.08	1.00	0.64	22	29
	Average	0.08	0.99	0.71	25	27
	Highest	0.10	0.89	0.59	26	28

Figure 5. Best quality factor found as a function of the resonance peak.

the experiments performed for resonance peaks lower than 700nm, there was no Quality Factor found by the evolutionary process.

The choice of present results of resonant peaks at 800nm and 900nm is because in the range between 600nm and 850nm is found the energy gap of the ternary alloy $Al_xGa_{1-x}As$. Therefore, at 900nm the cavity resonance is in a spectral region below the band gap of GaAs, presenting a low optical absorption. The optical absorption contributes strongly to the cavity linewidth broadening. Thus, the choice of a spectrum region with low optical absorption can provide an increased Q Factor of the sample, as observed in the results presented. A high transmittance in the resonance cavity indicates that the light can escape out easily in normal mode, minimizing the threshold of the laser device.

CONCLUSION

The optimization of semiconductor microcavities under uncertainties is presented in this paper. Microcavity structure has attracted the attention of scientist and engineers and has been applied to technological or purely scientific purpose. The optimization of microcavities parameters is a challenging task, mainly because some uncertainties are related to the growth process. These issues cause the synthesis of semiconductor nanodevices with undesirable layers thickness.

The optimization procedure proposed here was able to find satisfactory results, overcoming the known experimental solution. Also, the procedure found parameter sets that minimized the problem caused by the uncertainty. The results present high Q factor despite the uncertainties involved, which can assist the experts in the development of optimized structures. Microcavities structures with different resonance peaks were optimized (from 700nm and 2000nm). Also, we show that after 900nm the quality factor increases linearly as the resonance peak increase.

The next step of this work is the experimental synthesis of these devices, which is already under discussion and will be held soon.

ACKNOWLEDGEMENTS

The authors would like to thank CNPq, FAPEMIG, PRPq-UFMG and the Brazilian National Institute of Science and Technology on Semiconductor Nanodevices (INCT:DISSE) by financial support. We also would like to thanks Dr. Alain Andre Quivy for productive discussions about the growth of microcavities.

REFERENCES

[1] S. E. Morin, Q. Wu and T. W. Mossberg, “Cavity Quantum Electrodynamics at optical frequencies”, *Opt. Photon. News*, 3(8), 1992, 8-14.

[2] S. Haroche and D. Kleppner, “Cavity Quantum Electrodynamics”, *Phys. Today*, 42, 1989, 24-30.

[3] A. Imamöglu and R. J. Ram, “Semiconductor lasers without population inversion” *Opt. Lett*., 19, 1994, 1744-6.

[4] E. A. Cotta, “Semiconductor Microcavity: An Intrinsic Optical Transistor”, *IEEE ECS Trans*., 23(1) 2009, 545-51.

[5] C. de Matos, “Ultrafast coherent all-optical switching in quantum-well semiconductor microcavity”, *Elect. Lett.,* 36(1), 2000, 93-4.

[6] L. Ma, M. T. Rakher, M. J. Stevens, O. Slattery, K. Srinivasan and X. Tang, “Temporal correlation of photons following frequency up-conversion”, *Opt. Express,* 19(11), 2011, 10501-10.

[7] M. G. Banaee and J. F. Young, “Squeezed state generation in photonic crystal microcavities”, *Opt. Express,* 16(25), 2008, 20908-19.

[8] J. Kasprzak, *et. al*, “Bose-Einstein condensation of exciton polaritons”, *Nature,* 443, 2006, 409-14.

[9] E. A. Cotta and F. M. Matinaga, “Bistability double crossing curve effect in a polariton-laser semiconductor microcavity”, *Phys. Rev. B*, 76, 2007, 073308-11.

[10] Grant R. Fowles, *Introduction to Modern Optics,* 2nd Edition, Dover Pub., New York: 1989.

[11] Max Born and Emil Wolf, *Principles of Optics: Electromagnetic Theory of Propagation, Interference and Diffraction of Light*, 7th Edition, Cambridge University Press, Cambridge: 2003.

[12] W. Sellmeier, “Zur Erklärung der abnormen Farbenfolge im Spectrum einiger Substanzen”, *Annalen der Physik und Chemie*, 219, 1871, 272-82.

[13] S. Adachi, “Optical properties of $Al_xGa_{1-x}As$ alloys”, *Phys. Rev. B*, 38, 1988, 12345-52.

[14] C. H. Lin, J. M. Meese, M. L. Wroge and C. Weng, “Effect of GaAs/AlGaAs quantum-well structure on refractive index”, *IEEE Phot. Tech. Lett*., 6(5), 1994, 623-5.

[15] E. H. Li. "Refractive index of interdiffused AlGaAs/GaAs quantum well", *J. Appl. Phys.*, 82(12), 1997, 6251-8.

[16] R. J. Elliott, "Intensity of Optical Absorption by Excitons", *Phys. Rev.*, 108(6), 1957, 1384-9.

[17] Robert S. Knox., *Solid State Physics: Advances in Research and Applications and theory of Excitons*, Academic Press, New York: 1963.

[18] I. Bonalde, *et. al*, "Urbach tail, disorder, and localized modes in ternary semiconductors", *Phys. Rev. B*, 69(19), 2004, 195201-6.

[19] Z. Michalewicz, *Genetic algorithms + data structures = evolution programs*, Springer, New York: 1998.

APPENDIX A

Table I. Best results for resonance peak at 900nm, 1400nm and 2000nm. For each fitness strategy we present the ΔE, Q and F_i of all 10 structures. The last two lines show the mean and standard deviation.

800nm

Fitness:	Highest Evaluation			Average Evaluation			Lowest Evaluation		
Structure	ΔE (meV)	Q	F_i	ΔE (meV)	Q	F_i	ΔE (meV)	Q	F_i
1	0.0	1600	1600	0.0	1600	1600	0.0	1600	1600
2	4.7	1329	1072	4.6	1329	1072	4.8	1595	1276
3	4.2	1330	1089	3.7	1596	1341	3.9	1596	1330
4	1.2	1332	1256	1.2	1599	1508	1.2	1598	1508
5	5.8	1328	1022	5.2	1594	1255	5.2	1594	1255
6	6.0	1328	1014	7.0	1592	1171	7.0	1592	1171
7	4.7	1329	1072	4.1	1596	1319	4.3	1595	1307
8	2.5	1597	1414	1.7	1598	1466	1.7	1598	1466
9	2.5	1331	1178	2.7	1597	1401	2.7	1331	1167
10	1.7	1332	1222	1.9	1598	1453	1.9	1598	1452
Mean	3.3	1384	1194	**3.2**	**1570**	**1359**	3.3	1570	1353
St. Dev.	**1.9**	113	188.8	2.1	85	160.8	2.1	**84**	**146.6**

900nm

Fitness:	Highest Evaluation			Average Evaluation			Lowest Evaluation		
Structure	ΔE (meV)	Q	F_i	ΔE (meV)	Q	F_i	ΔE (meV)	Q	F_i
1	0.0	9000	9000	3.1	9020	7516	2.8	9018	7642
2	4.0	8974	7122	1.1	8993	8404	1.4	8991	8248
3	4.0	8974	7122	0	8999	8999	0.9	8994	8484
4	0.9	4497	4242	2.1	9014	7907	1.8	9012	8046
5	4.6	8970	6900	1.1	8993	8404	2.6	8983	7677
6	5.4	8965	6640	2.0	8987	7953	2.4	8984	7744
7	4.4	8971	6954	0.5	8997	8734	1.4	8991	8248
8	1.8	4494	4012	2.0	9013	7976	0.3	9002	8825
9	3.1	8980	7483	0.5	9003	8740	0.6	9004	8657
10	1.2	8992	8325	1.5	9010	8190	1.1	9007	8417
Mean	2.9	8081	6780	**1.4**	**9002**	**8283**	1.5	8998	8199
St. Dev.	1.8	1890	1570	**0.9**	**11**	459.0	2.4	12	**415**

2000nm

Fitness:	Highest Evaluation			Average Evaluation			Lowest Evaluation		
Structure	ΔE (meV)	Q	F_i	ΔE (meV)	Q	F_i	ΔE (meV)	Q	F_i
1	0.0	20000	20000	0.0	20000	20000	0.0	20000	20000
2	2.1	19932	11864	2.0	19935	12081	2.1	19933	11935
3	1.6	9973	6518	1.6	19949	13211	2.2	19928	11586
4	0.5	19984	17227	0.5	19984	17227	0.4	19988	17846
5	2.3	19925	11385	2.0	19934	12008	2.3	19927	11518
6	3.1	0	0	2.5	19919	11005	2.3	19925	11385
7	1.8	19942	12621	1.7	19944	12784	2.2	19930	11723
8	0.8	9987	7990	0.6	19982	16933	0.5	19984	17227
9	1.2	9980	7180	1.3	19959	14155	1.0	19967	15012
10	0.9	9985	7740	0.8	19975	15980	0.8	19974	15852
Mean	1.4	13971	10252	**1.3**	**19958**	**114538**	1.4	19955	14409
St. Dev.	0.9	6976	5706	**0.8**	**26**	**2882**	0.9	29	3202